



Interparticle arrival time analysis of bubble distributions in a dropshaft and hydraulic jump

Carlo Gualtieri (IAHR Member)

Hydraulic, Geotechnical and Environmental Engineering Department (DIGA), University of Napoli "Federico II", Via Claudio 21, I, 80125 Napoli, Italy.

Email: carlo.gualtieri@unina.it (corresponding author)

Hubert Chanson (IAHR Member)

School of Civil Engineering, The University of Queensland, Brisbane QLD 4072, Australia.

Email: h.chanson@uq.edu.au

ABSTRACT

The analysis of bubble clustering in air-water flows may provide some measure of the bubble-turbulence interactions. A cluster of bubbles is as a group of two or more bubbles, with a distinct separation from other bubbles. This paper compares the results of a clustering study in a dropshaft and in a hydraulic jump to point out differences/similarities between those complex turbulent flows. The clustering process was studied through the analysis of the interparticle arrival time of the bubbles. The results highlighted the presence of clustering in both bubbly flows due mostly to turbulent break-up. The range of bubbles sizes mainly affected by clustering was identified. The results showed that the bubbly flow in the dropshaft had a density of bubbles per unit flux larger than that in the hydraulic jump. Overall, the results demonstrated the relevance of the interparticle arrival times analysis in the study of bubbly flows.

Keywords: Air bubble entrainment, bubble clustering process dropshaft, hydraulic jump, interparticle arrival time analysis, laboratory experiments, Poisson distribution

1 Introduction

The study of air-water flows properties is of paramount importance in hydraulic structures. Two common energy dissipators, the dropshaft and the hydraulic jump, are characterized by significant air bubble entrainment. A dropshaft is a vertical structure connecting two channels with different invert elevations. This type of structure is commonly used in sewers and storm water systems. Despite the dropshaft being an ancient design used in Roman aqueducts, the studies of dropshaft hydraulics are limited (Rajaratnam *et al.* 1997), including the air-water flow properties (Gualtieri and Chanson 2004b, Chanson 2007). A hydraulic jump is a sudden transition from a supercritical flow into a subcritical flow. It is characterized by a sharp rise of the free-surface elevation associated with strong energy dissipation and air entrainment (Castro-Orgaz and Hager 2009). Recent studies on the air-water flows in the hydraulic jump included Mossa and Tolve (1998), Chanson and Brattberg (2000) and Murzyn *et al.* (2005), Gualtieri and Chanson (2007a) and Chanson and Gualtieri (2008), who carried out experiments in two channels with a geometric scaling of 2:1 and observed some scale effects with comparatively greater detrainment and lower dimensionless bubble count rates at low Reynolds numbers in the smaller model.

C.Gualtieri – H.Chanson

Interparticle arrival time analysis of bubble distributions in a dropshaft and hydraulic jump

Journal of Hydraulic Research, 2013, 51(3), 253-264 (DOI: 10.1080/00221686.2012.762430)

The complex interactions between the entrained air and turbulence may produce some bubble clustering. A cluster of bubbles is defined as a group of two or more bubbles with a distinct separation from the other bubbles before and after the cluster. A clustering analysis may provide some relevant insights about the interaction between turbulence and bubbly flow (Figueroa-Espinoza and Zenit 2005). Previous investigations studied the clustering process in plunging jets (Chanson *et al.* 2006), in stepped chutes (Chanson and Toombes 2002b), in the hydraulic jump (Gualtieri and Chanson 2007b, 2010) and in a dropshaft (Gualtieri and Chanson 2004a, 2007b, 2011).

This paper presents the comparative results of clustering analysis in a dropshaft and in a hydraulic jump. Despite they are used in different contexts and with different applications in water engineering, they are both complex turbulent shear flows characterized by strong energy dissipation. In these flows to identify a cluster structure an approach based upon the analysis of water chord between two adjacent air particles was applied in the past (Gualtieri and Chanson 2004a, 2007b, 2010, 2011). In this paper, a different approach based upon the interparticle arrival times (IAT) for the air bubbles was systematically for the first time applied to the above bubbly flows. Notably, the IAT analysis allows to identify not only the presence of clustering but even the range of particle sizes affected by clustering and ultimately the structure of each cluster and of the bubbly flow.

2 Experimental setups

The first group of experiments was performed in a large-size rectangular dropshaft built in marine plywood and perspex at the Hydraulics Laboratory of the University of Queensland (Australia). The dropshaft was 3.1 m high, 0.76 m wide and 0.75 long. The drop in invert was 1.7 m and the shaft pool was 1.0 m deep. The inflow and outflow channels were both horizontal, 0.5 m wide and 0.30 m deep. The upstream channel was open while the downstream conduit was covered and ended with a free overfall (Fig. 1 and 2). For a flow rate of 12 L/s, the free-falling jet impacted into the shaft pool (Fig. 2). Further details on the experimental data were presented in Gualtieri and Chanson (2004b).

The second group of experiments were performed at the University of Queensland in a horizontal channel, 3.2 m long and 0.25 m wide, with both bottom and sidewalls made by glass panels (Fig. 3). Preliminary clear water velocity measurements were carried out in the flume using a Prandtl-Pitot tube ($\varnothing=3.3$ mm). The results showed that the supercritical inflow was partially-developed for all investigated flow conditions (Table 2). In Table 2, W is the channel width, d_1 is the inflow (subscript 1) depth, V_1 is the inflow velocity, and $F_1 = V_1/(g \times d_1)^{0.5}$ is the inflow Froude number, whereas P/D means partially developed inflow conditions. The relative boundary layer thickness δ/d_1 was in the range from 0.5 to 0.6 depending upon the inflow conditions (Fig. 4). Further details on the experimental works were presented by Gualtieri and Chanson (2007a).

In both studies, the air-water flow properties were measured with a single-tip conductivity probe. It consisted of a sharpened rod (platinum wire $\text{Ø}=0.35$ mm) which was insulated except for its tip and set into a metal supporting tube (stainless steel surgical needle $\text{Ø}=1.42$ mm) acting as the second electrode. The measurement principle of conductivity probes is based upon the difference in electrical resistivity between air and water. The basic data processing yielded the air concentration or void fraction C , the bubble count rate F and the bubble chord time t_{ch-ab} . The void fraction C is the proportion of time that the probe tip is in the air. Past experience showed that the probe orientation with the flow direction has little effect on the void fraction accuracy provided that the probe support does not affect the flow past the tip. In the present study, the probe tip was aligned with the flow direction. The bubble count rate F is the number of bubbles impacting the probe tip. The measurement is sensitive to the probe tip size (Chanson and Toombes 2002a), bubble sizes, velocity and discrimination technique, particularly when the sensor size is larger than the smallest bubble sizes. The data accuracy is typically $\Delta C/C < 4\%$ for void fractions between 0.03 to 0.95. The bubble chord time t_{ch-ab} is defined as the time spent by the bubble on the probe tip.

The probe was excited by an electronic system designed with a response time less than 10 μs . In the dropshaft, the probe signal output was sampled at 25 kHz for a scanning duration $T_{scan} = 100$ s. Measurements were conducted at several cross-sections along the shaft centreline beneath the nappe impingement with depths ranging from 0.03 m to 0.25 m (Table 1). In the hydraulic jump, the probe sensor was scanned at 20 kHz for 45 s. The vertical position was controlled by a fine adjustment system with an accuracy of 0.1 mm. All the measurements were conducted on the channel centerline.

For some clustering analysis, the sampling rate must be at high-frequency : i.e., at least 10 to 20 kHz. Further the scan duration must almost one order of magnitude longer than that required for basic air water flow measurements (e.g. C and F) (Chanson and Toombes 2002b). The present experience in dropshaft and hydraulic jump flows suggested that a T_{scan} of 45 s was a minimum and T_{scan} of 100 s was preferable.

3 Clustering and interparticle arrival time analysis: Basic definitions

A *cluster* of bubbles is a group of two or more bubbles with a distinct separation from other bubbles (Gualtieri and Chanson 2004a, 2007b, 2010). In a cluster, the bubbles are close together and surrounded by a sizeable volume of water. The existence of clusters is generally related to turbulent break-up, coalescence, bubble wake interference and to other processes. The effect of the turbulence on the bubbles was found to alter their concentration field leading to a preferential accumulation at small scales, that is clustering, in regions of high vorticity. This confirms the intuition that

microbubbles would be subject to the same accumulation effect due to turbulence that had been found for heavy particles (Aliseda and Lasheras 2011). Air bubbles are trapped in large-scale vortical structures generated in the developing shear layers. As vortical structures are advected downstream, they grow up in size by vortex pairing and contribute to further clustering. Bubble wake interference is also important as pointed out by the clustering analysis carried out with the *near-wake* method (Gualtieri and Chanson 2010).

In the present study to identify a cluster the method based upon an *interparticle arrival time* (IAT) analysis was applied. The interparticle arrival time τ_{IA} is defined as the time between the arrival of two consecutive bubbles recorded by a probe sensor fixed in space. The distribution of τ_{IA} may provide some information about the occurrence or not of clustering within the flow structure. To determine the theoretical τ_{IA} distribution, the dispersed random flow has been modeled as a marked inhomogeneous Poisson process where individual bubbles act independently of each other (Edwards and Marx 1995a, 1995b). The Poisson process is described by the intensity function λ , which represents the expected number of particles to be sampled per unit time. Conversely, non-randomly-dispersed flows were defined as those whose τ_{IA} distributions do not follow Poisson statistics, associated with the occurrence of some bubble clustering (Edwards and Marx 1995a, 1995b, Martinez-Bazan *et al.* 2002, Aliseda and Lasheras 2011). In a randomly dispersed flow, the expected τ_{IA} distribution function is (Heinlein and Fritsching 2006):

$$f(\tau_{IA}) = \frac{\lambda^2 (T_{scan} - \tau_{IA}) \exp(-\lambda \tau_{IA})}{\lambda T_{scan} - 1 + \exp(-\lambda T_{scan})} \quad (1)$$

The intensity function can be estimated as $\lambda = N_{ab}/T_{scan}$, where N_{ab} is the number of sampled particles. As equation (1) describes an ideal randomly dispersed flow driven by a superposition of Poisson processes of bubble sizes, any deviations from equation (1) indicate the preferential accumulation of bubbles due to clustering, which may be quantified by a Chi-square analysis.

The IAT analysis is best conducted by breaking down the bubbly flow into narrow classes of particles of comparable sizes that are expected to have the same behaviour (Edwards and Marx 1995b). The simplest way is to divide the bubble population in terms of t_{ch-ab} . For the dropshaft, the IAT analysis was carried out in 12 points of measurement. The points with the highest C and/or F at each vertical elevation in the shaft pool were selected. These points are listed in Table 3 together with their air-water flow properties. They were located along the theoretical underwater nappe trajectory (Fig. 5). In Table 3 d_i is the thickness of the nappe at the impingement point in the dropshaft. For the hydraulic jump, the IAT analysis was carried out at the points with the highest C and/or F and at Y^* (Fig. 5), where Y^* represents the upper vertical boundary of the air diffusion layer

and is a meaningful parameter of air entrainment process (Gualtieri and Chanson 2007a). The number of points of measurement where the IAT analysis was performed were 12, 18 and 18 for F_1 equal to 6.5, 10.8 and 14.3, respectively. They are listed in Table 4 together with their C and F values. The column “*Comments*” indicates to whom parameter (C , F or Y^*) the measurement point is referring. At each location, both in the dropshaft and in the hydraulic jump, the detected bubbles were subdivided in 8 classes in terms of t_{ch-ab} (Table 5). The interparticle arrival times τ_{IA} were subdivided in 80 classes from 0 to 40 ms (size 0.5 ms).

4 Interparticle arrival times analysis: Results and discussion

4.1 Dropshaft

The analysis of interparticle arrival times τ_{IA} was first carried out considering all the recorded bubbles. Fig. 6 presents the results of IAT analysis in the dropshaft at $x=150$ mm and $z=30$ mm and at $x=155$ mm and $z=150$ mm, respectively. The experimental data are compared with equation (1) and both the expected deviations and Chi-square values are also provided. Both figures showed that the experimental distribution of bubbles was different from that expected for a random process. Bubbles with τ_{IA} less than from 1.5 to 2.0 ms did not show a true random behavior. These bubbles have a frequency higher than that predicted by Poisson law. Hence, some clustering occurred. Further the difference between experimental and theoretical data decreased with the increasing depth below the water surface.

The IAT analysis in the dropshaft was also carried out dividing the whole bubbles population into 8 sub-classes of bubbles with similar values of the air chord time t_{ch-ab} (Table 5). Fig. 7 presents results in the dropshaft for two chord time sub-classes (or bins) at the point with $x=150$ mm and $z=30$ mm, already presented in Fig. 6. In Fig. 7, the sub-classes were 1 and 3 for which the air chord time ranged from 0 to 0.5 ms and from 1.5 to 3.0 ms, respectively (Table 5). In both classes, the τ_{IA} experimental distributions differed substantially in shape from the theoretical distribution, i.e. equation (1). For example, in Fig. 7(a) (Class 1), the expected deviation of a random bubbly mixture from the theoretical curve was about +/- 15%, whereas the four shortest τ_{IA} classes (i.e. 0–0.5, 0.5–1.0, 1.0–1.5 and 1.5–2.0 ms) had a population that was about 9.0, 5.5, 4.0 and 2.7 times the expected value, respectively. These large deviations indicated that bubbles with short τ_{IA} were in the bubbly flow with higher probability than it could be expected in a randomly distributed bubbly flow. In Fig. 7(b) (Class 3), the expected deviation from the theoretical curve was about +/- 27%, whereas the

four shortest τ_{IA} classes had a population that was about 10.0, 6.5, 7.0 and 5.0 times the expected value, respectively. In Fig. 7(a) (Class 1), the frequency of the short τ_{IA} was larger than in Fig. 6(b) (Class 3), but the deviations from Poisson distribution were smaller. Also, that, for both classes, the difference between experimental data and Poisson distribution decreased to zero with the increasing τ_{IA} .

Fig. 8 presents the data in the dropshaft for Class 1 at the point with $x=115$ mm and $z=250$ mm, i.e. at the deepest measurement point in the shaft pool. This allowed a comparison between the same class, namely Class 1, at two different depths. In Fig. 8, the expected deviation of a random bubbly mixture from the theoretical curve was about $\pm 35\%$, whereas the four shortest τ_{IA} classes had a population that was about 16.5, 10.0, 12.0 and 7.0 times the expected value, respectively. A comparison between Fig. 7 and 8 suggests that the frequency of bubbles with very short τ_{IA} was higher close to the water surface, where turbulent shear was the largest. The relative differences from the Poisson distribution were highest for the largest depth (i.e. $z=250$ mm). Overall, the results in the dropshaft showed that the experimental distributions of τ_{IA} were significantly different from the Poisson distribution for τ_{IA} between 0.0 and 5–7 ms with the largest values at $z=250$ mm.

4.2 Hydraulic jump

As for the dropshaft, the IAT analysis for the hydraulic jump was first carried out considering all the recorded bubbles. Fig. 9 presents the results of the analysis for the hydraulic jump at the elevation with F_{max} at a dimensionless distance from the jump toe $(x-x_1)/d_1=4.17$ and 3.91 for $F_1=6.51$ and 10.8, respectively. Fig. 10, on the left, shows the results for the hydraulic jump at Y^* and at $(x-x_1)/d_1=27.3$ for $F_1=10.8$. Fig. 10, on the right, presents the results at $(x-x_1)/d_1=4.20$ for the elevation with F_{max} and $F_1=14.3$. Fig. 11 presents results for $F_1=14.3$ at the elevation with F_{max} and at different distances from the jump toe, e.g. $(x-x_1)/d_1=29.4$ and 42.0. Finally, Fig. 12 shows the data for $F_1=14.3$ and at $(x-x_1)/d_1=54.6$, but for different elevations. i.e. $y/d_1=5.601$ and 9.382, corresponding to the elevation with F_{max}/C_{max} and of Y^* . In any case, the experimental data are compared with equation (1) and both the expected deviations and Chi-square values are also provided.

All figures showed that the distribution of the air bubbles was different from that expected for a random process. Bubbles with τ_{IA} from less than from 1.5 to 7.5 ms had a frequency higher than that predicted by Poisson law. First the deviations from Poisson distribution were larger at larger Froude number at the same distance from the jump toe and at the elevation with the maximum F (Fig. 9 and Fig. 10(b)). This demonstrated an influence of F_1 on the rate of clustering confirming previous findings obtained with a different technique for cluster identification (Gualtieri and Chanson 2010). Second, for the same Froude number, i.e. $F_1=14.3$, and at the elevation with F_{max} , the deviation from

Poisson distribution for smaller τ_{IA} was the largest close to the jump toe. Also it decreased with the increasing distance from this (Fig. 10(b), Fig. 11, Fig. 12(a)). Third, again for $F_1=14.3$, and at the same distance from the jump toe, i.e. $(x-x_1)/d_1=54.6$, the deviation from Poisson distribution was larger at the elevation with F_{max} than with Y^* (Fig. 12).

As for the dropshaft, the analysis in the hydraulic jump was also carried out dividing the whole bubbles population into 8 sub-classes of bubbles with similar t_{ch-ab} values (Table 5).

Fig. 13 presents the results in the hydraulic jump for two chord time sub-classes for $F_1=14.3$ at $(x-x_1)/d_1=8.40$ and $y/d_1=1.399$, which is the elevation with C_{max} and F_{max} . In Fig. 13, the sub-classes were 1 and 2 where t_{ch-ab} ranged from 0 to 0.5 ms and from 0.5 to 1.5 ms, respectively (Table 5). For both classes the experimental and theoretical distributions were different.

For example, in Fig. 13(a) (Class 1), the expected deviation of a random bubbly mixture from the theoretical curve was about +/- 15%, whereas the eight shortest τ_{IA} classes (i.e. 0–0.5, 0.5–1.0, 1.0–1.5, 1.5–2.0, 2.0–2.5, 2.5–3.0, 3.0–3.5, 3.5–4.0 ms) had a population that was about 4.8, 4.4, 3.1, 2.6, 2.7, 2.4, 2.2 and 2.1 times the expected value, respectively. These large deviations indicated that bubbles with short τ_{IA} were present in the flow with higher probability than it could be expected in a randomly distributed bubbly flow. In Fig. 13(b) (Class 2), the expected deviation from the theoretical curve was about +/- 18%, whereas the eight shortest τ_{IA} time classes had a population that was about 4.7, 4.7, 3.3, 2.9, 2.2, 2.3, 1.6 and 1.9 times the expected value, respectively. Comparing with the dropshaft, the deviations were smaller. Notably, in Fig. 13(a) (Class 1), the frequency of the short τ_{IA} was larger than in Fig. 13(b) (Class 2), but the deviations from Poisson distribution were smaller. Also, for both classes, the difference between experimental data and Poisson distribution decreased to zero with the increasing τ_{IA} . This trend was consistent with that observed in the dropshaft.

4.3 Comparative analysis between dropshaft and hydraulic jump. Discussion

A comparative discussion of the results from the IAT analysis in the dropshaft and in the hydraulic jump pointed out some similarities and differences between these bubbly flows.

The analysis was first conducted considering all the recorded bubbles. Herein, in both cases significant differences between the experimental and theoretical distributions were observed. Bubbles with short τ_{IA} had a frequency higher than that predicted by Poisson law. At the intermediate τ_{IA} the frequency was below that of the Poisson law and finally the difference between experimental data and Poisson distribution decreased to zero with the increasing τ_{IA} . Hence, the presence of clustering was inferred by the increase of the frequency of air bubbles with short τ_{IA} . In the dropshaft, a frequency larger than that of Poisson law was observed for bubbles with τ_{IA} less than

from 1.5 to 2.0 ms. In the hydraulic jump this was observed for bubbles with τ_{IA} less than from 1.0 (Fig. 10(b)) to 7.5 ms (Fig. 10(a)).

Furthermore in both flows, the analysis was carried out dividing the whole bubbles population into 8 sub-classes of bubbles with similar t_{ch-ab} (Table 5). Again, in both turbulent flows, large deviations from Poisson distribution were observed. These deviations were observed for bubbles with τ_{IA} less than from 7.5 to 15.0 ms and less than from 10.0 to 12.0 ms in the dropshaft and in the hydraulic jump, respectively. The largest deviations were observed in the dropshaft close to the water surface ($z=30$ mm) for the smallest bubbles (Class 1), where the highest frequency was 0.15 (Fig. 7(a)). In the hydraulic jump, the largest frequency was 0.08 and it occurred for the smallest bubbles (Class 1) near to the jump toe in the hydraulic jump at $F_1=14.3$ (Fig. 13(a)). In both flows the frequency of bubbles with very short τ_{IA} decreased with the increasing bubble chord time, i.e. from Class 1 to Class 2 or 3, and with the depth below the water surface in the dropshaft and the distance from the jump toe in the hydraulic jump.

To better highlight similarities or differences between the bubbly flows in the dropshaft and in the hydraulic jump the effects of the distance from the impingement point/jump toe and of the Reynolds number on the clustering process were systematically investigated.

The analysis of the effect of the distance from the impingement point/jump toe on the clustering process was first carried out considering all the recorded bubbles. Fig. 14 presents the distribution with the distance from the impingement point in the dropshaft and the jump toe in the hydraulic jump of the PDF for all the recorded bubbles with τ_{IA} from 0 to 0.5 ms (Fig. 14(a)) and from 1.0 to 1.5 ms (Fig. 14(b)). In these plots, the point with the maximum F was considered. First, in both flows the PDF decreased with the increasing dimensionless distance z/d_1 for the dropshaft and $(x-x_1)/d_1$ for the hydraulic jump, where the PDF decreased with the decreasing inflow Froude number F_1 at a given $(x-x_1)/d_1$. Second, the decrease was more rapid for the hydraulic jump at low F_1 . Third, independently of the distance, the frequency of bubbles with short τ_{IA} was in the dropshaft generally larger than in the hydraulic jump. The analysis of the effect of the distance from the impingement point/jump toe was then repeated for the bubbles belonging to Class 1 (Table 5), i.e. the bubbles with the smallest air chord time. A similar trend was generally observed. After all the trend presented in Fig. 14 suggested that in both flows the largest values of the PDF were observed where turbulent shear stresses were very large, i.e. close below the impingement point in the dropshaft and near to the jump toe in the hydraulic jump at the largest F_1 .

The analysis of the effect of the Reynolds number on the clustering process was first carried out considering all the recorded bubbles. Fig.15 presents the distribution with R of the PDF for all the bubbles with τ_{IA} from 0 to 0.5 ms, from 0.5 to 1.0 ms and from 1.0 to 1.5 ms. The data for the

dropshaft are those with the full symbols for $R=24000$. Table 6 lists the value of the Reynolds number for both flows. The Reynolds number for the flow in the dropshaft was calculated using the velocity and the thickness of the nappe at the impingement point (Gualtieri and Chanson 2004b). The data demonstrated that for a similar R the flow in the dropshaft had a frequency of bubbles with very short τ_{IA} larger than the flow in the hydraulic jump. This indicated that for a similar level of turbulence, the bubbly flow in the dropshaft had a structure where bubbles very close to each other are more frequent than in the hydraulic jump flow. In other words, for a similar level of turbulence, the density of bubbles per unit flux in the dropshaft flow was larger than that in the hydraulic jump. Moreover, in the hydraulic jump the bubbly flow had a greater density of bubbles per unit flux at high R (and F_1). The analysis of the effect of the Reynolds number on the clustering process was then repeated with similar results for the bubbles belonging to Class 1 (Table 5).

Overall, these results suggested that the main mechanism responsible for clustering in both flows was turbulent break-up and the structure of the bubbly flow in the dropshaft had a larger density of bubbles per unit flux.

4.4 Comparison with previous studies on clustering. Discussion

The clustering process is studied in many areas of environmental sciences, physics of the atmosphere, meteorology and oceanography as well as in mechanical and civil engineering. The literature on clustering encompasses some studies ranging from experimental works to numerical investigations and theory developments. Different approaches were applied to identify a cluster structure. One approach is based upon the analysis of water chord between two adjacent air particles. If two subsequent bubbles are closer than a characteristic time/length scale, they can be considered as a cluster. This time/length scale may be related to the water chord statistics, such as the mean or the median t_{ch-w} , or to the bubble size itself, as bubbles within that distance are in the near-wake of the leading particle. These methods were applied to the dropshaft and to the hydraulic jump (Table 7) (Gualtieri and Chanson 2004a, 2007b, 2010, 2011). However, these methods provided only some general features of the clustering process, such as the number of clusters, of clustered bubbles and of bubbles belonging to cluster structures in each point of measurement, whereas the IAT analysis allows also to identify the range of particle sizes affected by clustering. Note that the IAT analysis was also already applied in the last decade outside the field of hydraulic structures as for the characterization of clustering in turbulent jets (Table 7) (Martinez-Bazan *et al.* 2002, Milenković *et al.* 2007, Calzavarini *et al.* 2008) and in sprays (Heinlein and Fritsching 2006).

The above methods are indeed complementary. The approach based upon the analysis of water chord between two adjacent air particles offers a general picture of the clustering process, whereas

the IAT analysis provides detailed information about the structure of each cluster, the range of bubbles sizes affected by clustering and ultimately the structure of the bubbly flow. In any case, both methods highlighted that the formation of cluster structures is a common characteristic in dropshaft and hydraulic jumps flows and that a large proportion of the bubbles travel within cluster structures, whereas only the second approach allowed to point out that the bubbly flow in the shaft pool had a structure where bubbles very close to each other are more frequent than the hydraulic jump flow.

5 Conclusion

Bubbles clustering may be regarded as some small-scale in-homogeneities of the bubbles spatial distribution in a turbulent flow. Hence clustering studies are mostly aimed at studying the interactions between bubbles and large-scale vortices and ultimately to better characterize some complex turbulent air-water flows. The paper presented the results of a comparative clustering analysis conducted in two energy dissipators that are characterized both by some substantial air entrainment: a rectangular dropshaft corresponding to a near full-scale industrial facility and a hydraulic jump.

For the clustering analysis, an approach based upon the interparticle arrival times τ_{IA} for the air bubbles was applied. This analysis involved the bubbles chord times, and it is believed to be applied systematically for the first time to the bubbly flows in a dropshaft and in a hydraulic jump. The distributions of τ_{IA} were compared to the Poisson distribution characterizing a random process.

First, in both cases a significant deviation from Poisson law was observed at the smaller τ_{IA} , inferring the presence of cluster structures consisting of small bubbles. The results confirmed that turbulence significantly modified the concentration field of the bubbles leading to preferential accumulation at small scales, that is clustering, in both flows. Hence in both flows the interactions between entrained air bubbles and turbulent structures cannot be ignored. These interactions are likely to significantly contribute to the overall energy dissipation.

Second, in the dropshaft the difference between experimental and theoretical data decreased with the increasing depth below the water surface and with the increasing t_{ch-ab} . In the hydraulic jump the deviation from Poisson distribution increased with the increasing inflow Froude number F_1 at the same distance from the jump toe and at the elevation with the maximum bubble count rate. This demonstrated an influence of F_1 on the rate of clustering. Moreover, for the same F_1 , the deviation from Poisson distribution for smaller τ_{IA} was the largest close to the jump toe and it decreased with the increasing distance from the jump toe. Overall, the clustering process was larger close to the water surface in the shaft pool, as well as close to the jump toe, where large turbulent shear stresses took place.

Third, the largest value of cluster frequency was observed in the dropshaft, whereas in the hydraulic jump bubbles with larger τ_{IA} were affected by clustering. This result was also confirmed by the IAT analysis conducted dividing the whole bubbles population into 8 sub-classes of bubbles with similar values of the air chord time. This type of analysis allowed to identify the range of bubbles sizes affected by clustering indicating that clustering involved mainly the small bubbles with shorter similar t_{ch-ab} in both the facilities.

Finally, the data demonstrated that for a similar level of turbulence the flow in the dropshaft had a frequency of clustered bubbles with very short τ_{IA} larger than the flow in the hydraulic jump. Hence, the bubbly flow structure in the dropshaft had a density of bubbles per unit flux larger than in the hydraulic jump flow. This suggests a stronger level of interaction between air bubbles and turbulent flow in the dropshaft. Moreover, in the hydraulic jump the bubbly flow had a greater density of bubbles per unit flux at high R (and F_1).

Overall, the experimental results demonstrated the relevance of the interparticle arrival times analysis in the study of bubbly flows. This analysis confirmed some findings obtained with a different method for clusters identification (Gualtieri and Chanson 2004a, 2007b, 2010, 2011), but even provided new insights into the level of interaction between air bubbles and turbulent flow, the structure of clusters and ultimately of the bubbly flows in the dropshaft and the hydraulic jump.

Acknowledgements

The first author acknowledges the financial support from the Exchange Program for Professors and Researchers of the University of Napoli *Federico II* for the year 2003 and 2006 and the preliminary work carried out by his former student O.Casoria.

Notation

C = void fraction [-]

d_i = thickness of the nappe at the impingement point in the dropshaft [m]

d_1 = channel depth in the hydraulic jump [m]

F = bubble count rate [Hz]

F_{scan} = scanning rate [Hz]

F_1 = Froude number [-]

L = dropshaft length [m]

N_{ab} = number of sampled particles [-]

Q = flowrate in the dropshaft [L/s]

R = Reynolds number [-]

t_{ch-ab} = air chord time [s]

t_{ch-w} = water chord time [s]

T_{scan} = scanning duration [s]

V_1 = inflow velocity in the hydraulic jump [m/s]

W = channel width in the hydraulic jump [m]

x = streamwise distance from the outflow channel, positive upstream, in the dropshaft [m]

x = streamwise distance from gate in the hydraulic jump [m]

x_1 = streamwise distance of impingement point from gate in the hydraulic jump [m]

y = vertical elevation, positive upward, in the hydraulic jump [m]

Y^* = upper vertical boundary of air diffusion layer in the hydraulic jump [m]

z = vertical distance from the pool free-surface, positive downward, in the dropshaft [m]

Greek symbols

δ = boundary layer thickness [m]

λ = intensity function [Hz]

τ_{IA} = interparticle arrival time [s]

Subscripts

max = maximum

scan = scanning

1 = refers to inflow condition

References

- Aliseda, A., Lasheras, J.C. (2011). Preferential concentration and rise velocity reduction of bubbles immersed in a homogeneous and isotropic turbulent flow. *Phys. Fluids* 23, 093301.
- Calzavarini, E., van den Berg, T.H., Luther, S., Toschi, F., Lohse, D. (2008). Quantifying microbubble clustering in turbulent flow from single-point measurements. *Phys. Fluids* 20, 040702.
- Chanson, H. (2007). Air Entrainment Processes in Rectangular Dropshafts at Large Flows. *J. Hydraulic Res.* 45(1), 42–53.

- Chanson, H., Brattberg, T. (2000). Experimental study of the air-water shear flow in a hydraulic jump. *Int. J. Multiphase Flow* 26(4), 583–607.
- Chanson H, Toombes L. (2002a). Experimental study of gas–liquid interfacial properties in a stepped cascade flow. *Environ. Fluid Mech.* 2(3), 41–263.
- Chanson, H., Toombes, L. (2002b). Air-Water flows down stepped chutes: Turbulence and flow structure observations. *Int. J. Multiphase Flow* 28(11), 1737–1761.
- Chanson, H., Aoki, S., Hoque, A. (2006). Bubble entrainment and dispersion in plunging jet flows: Freshwater versus seawater. *J. Coastal Res.* 22(3), 664–677.
- Chanson, H., Gualtieri, C. (2008). Similitude and scale effects of air entrainment in hydraulic jumps. *J. Hydraulic Res.* 46(1), 35–44.
- Edwards, C.F., Marx, K.D. (1995a). Multipoint statistical structure of the ideal spray, Part I: Fundamental concepts and the realization density. *Atomization and Sprays* 5, 435–455.
- Edwards, C.F., Marx, K.D. (1995b). Multipoint statistical structure of the ideal spray, Part II: Evaluating steadiness using the interparticle time distribution. *Atomization and Sprays* 5, 457–505.
- Figuroa-Espinoza, B., Zenit, R. (2005). Clustering in high Re monodispersed bubbly flows. *Phys. Fluids* 17, 091701.
- Gualtieri, C., Chanson, H. (2004a). Clustering process and interfacial area analysis in a large-size dropshaft. *Advances in Fluid Mechanics* 5, 415–424, A. Mendes, M. Rahman, C.A. Brebbia, eds. WIT Press, Southampton UK.
- Gualtieri, C., Chanson, H. (2004b). Analysis of air bubbles probability distribution functions in a large-size dropshaft. Proc. Int. Conf. 3rd *International Symposium on Two-Phase Flow Modelling and Experimentation (ISTP 2004)*, Pisa, 1–8, G.P.Celata, P.Di Marco, A.Mariani, R.K.Sha.
- Gualtieri, C., Chanson, H. (2007a). Experimental analysis of Froude number effect on air entrainment in hydraulic jumps. *Environ. Fluid Mech.* 7(3), 217–238.
- Gualtieri, C., Chanson, H. (2007b). Clustering process analysis in a large-size dropshaft and in a hydraulic jump. Proc. 32nd *IAHR Congress Venice*, C1(b), 1–11.
- Gualtieri, C., Chanson, H. (2010). Effect of Froude number on bubble clustering in a hydraulic jump. *J. Hydraulic Res.* 48(4), 504–508.

- Gualtieri, C., Chanson, H. (2011). Bubble clustering in a large-size dropshaft. Comparative analysis of different cluster criteria. Proc. 34nd IAHR Congress Brisbane, 1–8.
- Heinlein, J., Fritsching, U. (2006). Droplet clustering in sprays. *Exp. Fluids* 40, 464–472.
- Martinez-Bazan, C., Montanes, J.L., Lasheras, J.C. (2002). Statistical description of the bubble cloud resulting from the injection of air into a turbulent water jet. *Int. J. Multiphase Flow* 28, 597–615.
- Milenković, R.Ž, Sigg, B., Yadigaroglu, G. (2007). Bubble clustering and trapping in large vortices. Part 1: Triggered bubbly jets investigated by phase-averaging. *Int. J. Multiphase Flow* 33, 1088–1110.
- Mossa, M., Tolve, U. (1998). Flow visualization in bubbly two-phase hydraulics jump. *J. Fluids Eng.* 120, March, 160–165.
- Murzyn, F., Mouaze, D., Chaplin, J.R. (2005). Optical fibre probe measurements of bubbly flow in hydraulic jumps. *Int. J. Multiphase Flow* 31(1), 141–154.
- Castro-Orgaz, O., Hager, W.H. (2009). Classical hydraulic jump: basic flow features. *J. Hydraulic Res.* 47(6), 744–754.
- Rajaratnam, N., Mainali, A., Hsung, C.Y. (1997). Observations on flow in vertical dropshafts in urban drainage systems. *J. Envir. Eng.* 123(5), 486–491.

Table 1 – Dropshaft experiments : position of the measurement points

Depth z – mm	x – mm
30	60-205
50	85-505
80	80-205
110	75-200
150	70-205
200	75-205
250	60-170

Table 2 – Experimental flow conditions in the hydraulic jump

Reference	W – m	d_1 – m	V_1 – m/s	F_1	Comments
Present study	0.25	0.012 to 0.0138	2.23 to 4.87	6.5 to 14.3	Conductivity probe (single tip, 0.35 mm inner electrode), PD inflow conditions

Table 3 – Measurement points selected for the IAT analysis in the dropshaft

Depth z – mm	z/d_1	x/L	C	F – Hz
30	7.23	0.199	0.543	242.3
30	7.23	0.205	0.554	236.9
50	12.05	0.192	0.602	264.5
80	19.28	0.179	0.570	251.1
110	26.52	0.185	0.375	219.9
110	26.52	0.192	0.378	207.6
150	36.16	0.179	0.338	159.6
150	36.16	0.205	0.332	178.5
200	48.21	0.159	0.264	128.7
200	48.21	0.172	0.233	133.2
250	60.26	0.146	0.132	76.5
250	60.26	0.152	0.133	74.1

Table 4 – Measurement points selected for the IAT analysis in the hydraulic jump

F_1	Distance ($x-x_1$)/ d_1	y/d_1	Comments	C	$F -$ Hz	F_1	Distance ($x-x_1$)/ d_1	y/d_1	Comments	C	$F -$ Hz
6.5	4.17	1.596	F_{\max} and Y^*	0.096	28.0	10.8	39.06	4.816	F_{\max}	0.040	25.7
6.5	8.33	2.846	C_{\max}	0.108	13.0	10.8	39.06	8.723	Y^*	0.064	17.9
6.5	8.33	3.471	Y^*	0.144	15.1	10.8	50.78	9.504	F_{\max}	0.041	12.8
6.5	8.33	3.888	F_{\max}	0.526	20.4	10.8	50.78	11.066	C_{\max}	0.249	16.6
6.5	12.50	2.846	C_{\max}	0.030	8.4	14.3	4.20	0.979	F_{\max}	0.165	173.4
6.5	12.50	4.721	Y^*	0.098	8.7	14.3	4.20	1.399	C_{\max}	0.529	103.0
6.5	12.50	5.138	F_{\max}	0.427	16.4	14.3	4.20	2.239	Y^*	0.355	45.6
6.5	16.67	3.263	C_{\max} and F_{\max}	0.016	4.1	14.3	8.40	1.399	C_{\max} and F_{\max}	0.343	177.8
6.5	16.67	4.721	Y^*	0.013	3.0	14.3	8.40	3.500	Y^*	0.246	34.0
10.8	3.91	0.910	F_{\max} and Y^*	0.088	98.8	14.3	16.81	1.819	F_{\max}	0.216	174.2
10.8	7.81	1.301	F_{\max}	0.224	138.2	14.3	16.81	2.239	C_{\max}	0.250	152.5
10.8	7.81	1.691	C_{\max}	0.271	53.9	14.3	16.81	4.761	Y^*	0.182	30.3
10.8	7.81	2.863	Y^*	0.233	33.3	14.3	29.41	2.239	F_{\max}	0.119	119.0
10.8	11.72	1.301	F_{\max}	0.170	130.7	14.3	29.41	3.920	C_{\max}	0.149	85.0
10.8	11.72	2.277	C_{\max}	0.249	65.8	14.3	29.41	7.282	Y^*	0.094	22.0
10.8	11.72	3.254	Y^*	0.240	31.1	14.3	42.02	3.500	F_{\max}	0.080	69.0
10.8	15.63	1.691	F_{\max}	0.181	122.6	14.3	42.02	6.021	C_{\max}	0.101	49.4
10.8	15.63	2.863	C_{\max}	0.227	57.9	14.3	42.02	9.382	Y^*	0.047	16.3
10.8	15.63	4.426	Y^*	0.153	24.0	14.3	54.62	5.601	C_{\max} and F_{\max}	0.074	43.2
10.8	27.34	3.254	F_{\max}	0.073	47.5	14.3	54.62	9.382	Y^*	0.056	20.8
10.8	27.34	3.645	C_{\max}	0.074	43.8	14.3	67.23	11.063	F_{\max}	0.059	21.2
10.8	27.34	6.379	Y^*	0.050	14.3	14.3	67.23	13.584	Y^*	0.073	16.4
10.8	39.06	4.426	C_{\max}	0.036	24.6						

Table 5 – Classes of bubbles for the IAT analysis in both the dropshaft and the hydraulic jump

Class	Air chord time t_{ch-ab} – ms
1	[0.0, 0.5]
2	[0.5, 1.5]
3	[1.5, 3.0]
4	[3.0, 5.0]
5	[5.0, 7.5]
6	[7.5, 10.0]
7	[10.0, 15.0]
8	>15

Table 6 – Reynolds number R for the dropshaft and the hydraulic jump

	R
Droshaft	24000
Hydraulic jump – $F_1=6.51$	26800
Hydraulic jump – $F_1=10.8$	48800
Hydraulic jump – $F_1=14.3$	58000

Table 7 – Experimental studies about clustering analysis in air-water flows

Reference	Air-water flow	Clustering analysis method
Martinez-Bazan <i>et al.</i> 2002	Turbulent jet	Phase Doppler Particle Analyzer (PDPA), Interparticle arrival times τ_{IA} (IAT) analysis
Chanson and Toombes 2002b	Stepped chute	Double tip probe, t_{ch-w} compared to the mean of t_{ch-w}
Gualtieri and Chanson 2004a	Dropshaft	Single tip probe, t_{ch-w} compared to the mean of t_{ch-w}
Heinlein and Fritsching 2006	Spray	Phase Doppler Particle Analyzer (PDPA), Interparticle arrival times τ_{IA} (IAT) analysis
Chanson <i>et al.</i> 2006	Plunging jet	Single tip probe, t_{ch-w} compared to the t_{ch-ab} of the leading bubble
Milenković <i>et al.</i> 2007	Turbulent jet	Flow visualization, Interparticle arrival times τ_{IA} (IAT) analysis
Gualtieri and Chanson 2007b	Dropshaft and Hydraulic Jump	Single tip probe, t_{ch-w} compared to (1) the mean and (2) the median of t_{ch-w}
Calzavarini <i>et al.</i> 2008	Turbulent jet	Hot-film anemometry probe, Interparticle arrival times τ_{IA} (IAT) analysis
Gualtieri and Chanson 2010	Hydraulic Jump	Single tip probe, t_{ch-w} compared to (1) the median of t_{ch-w} and (2) the t_{ch-ab} of the leading bubble
Gualtieri and Chanson 2011	Dropshaft	Single tip probe, t_{ch-w} compared to (1) the mean, (2) the median of t_{ch-w} and (3) the t_{ch-ab} of the leading bubble
Aliseda and Lasheras 2011	Turbulent jet	Phase Doppler Particle Analyzer (PDPA), Flow visualization, Bubble concentration
Present study	Dropshaft and Hydraulic Jump	Interparticle arrival times τ_{IA} (IAT) analysis

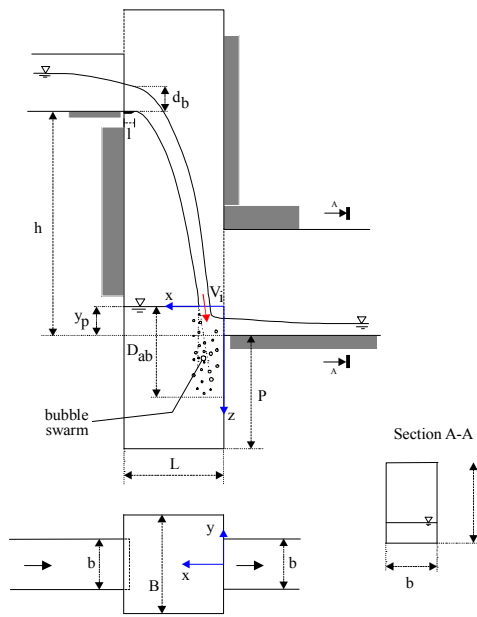


Fig. 1 – Sketch of a rectangular dropshaft

Fig. 2 – Dropshaft in operation with $Q=12$ L/s

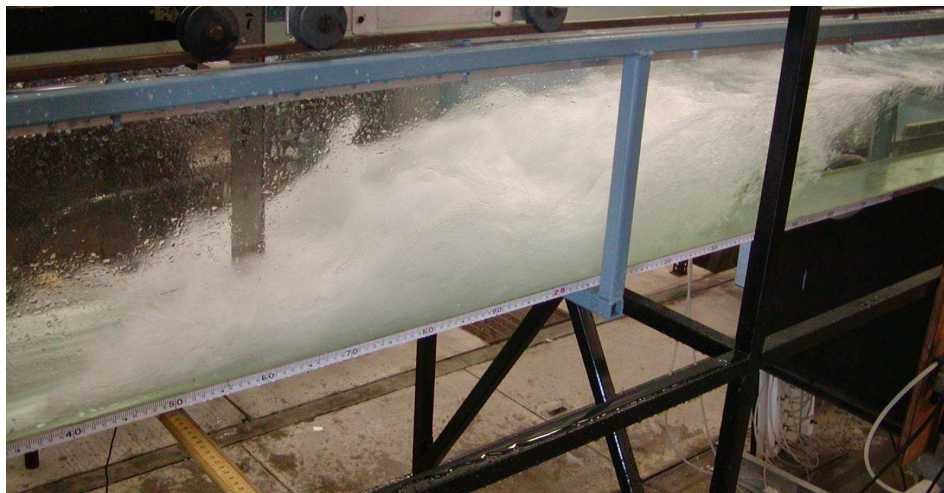


Fig. 3 – The hydraulic jump at $F_1=14.3$

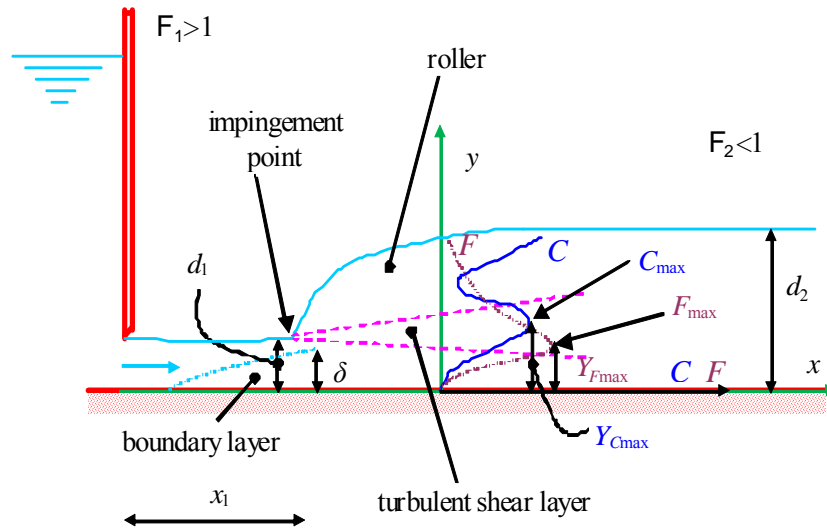


Fig. 4 – Sketch of hydraulic jump flow with partially-developed inflow conditions

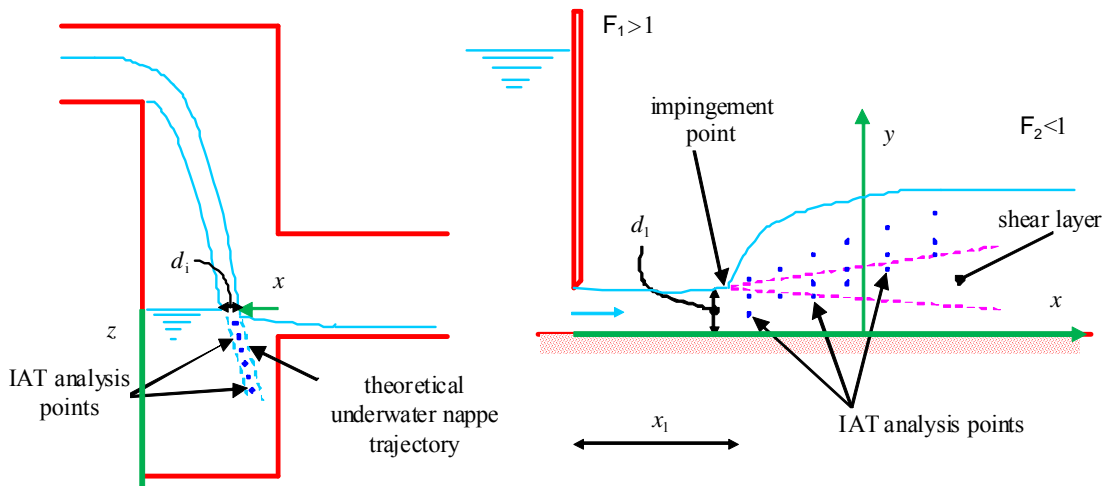


Fig. 5 – Sketch of the points where the IAT analysis was carried out for the dropshaft and the hydraulic jump flows

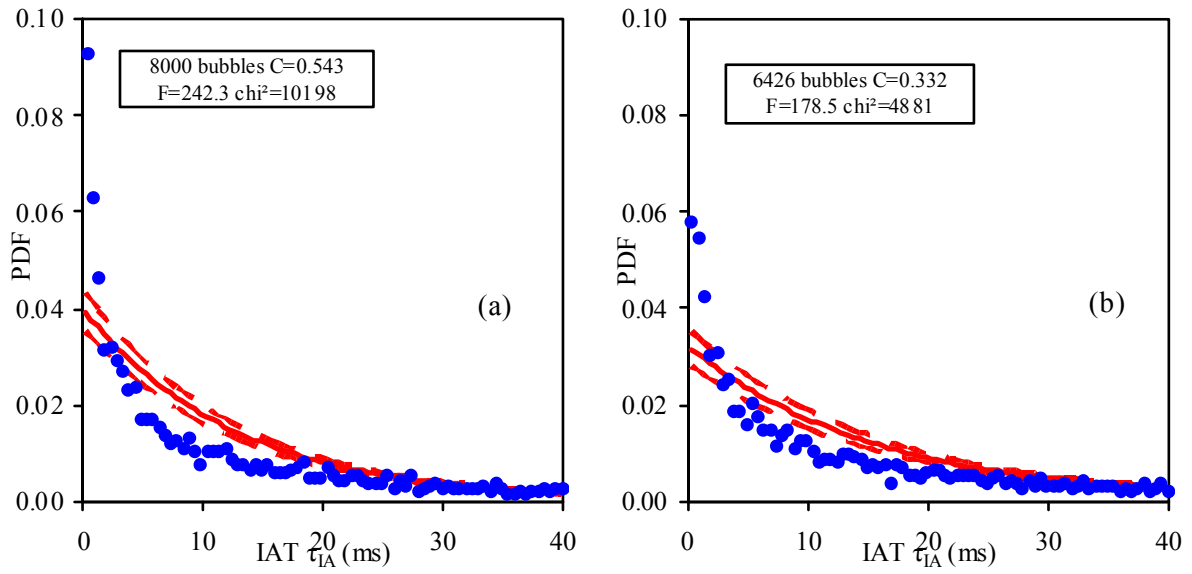


Fig. 6 – Interparticle arrival time analysis in the dropshaft at (a) $x=150$ mm and $z=30$ mm and (b) $x=155$ mm and $z=150$ mm, (●) experimental data, (—) Poisson distribution, (dashed line) lower/upper range

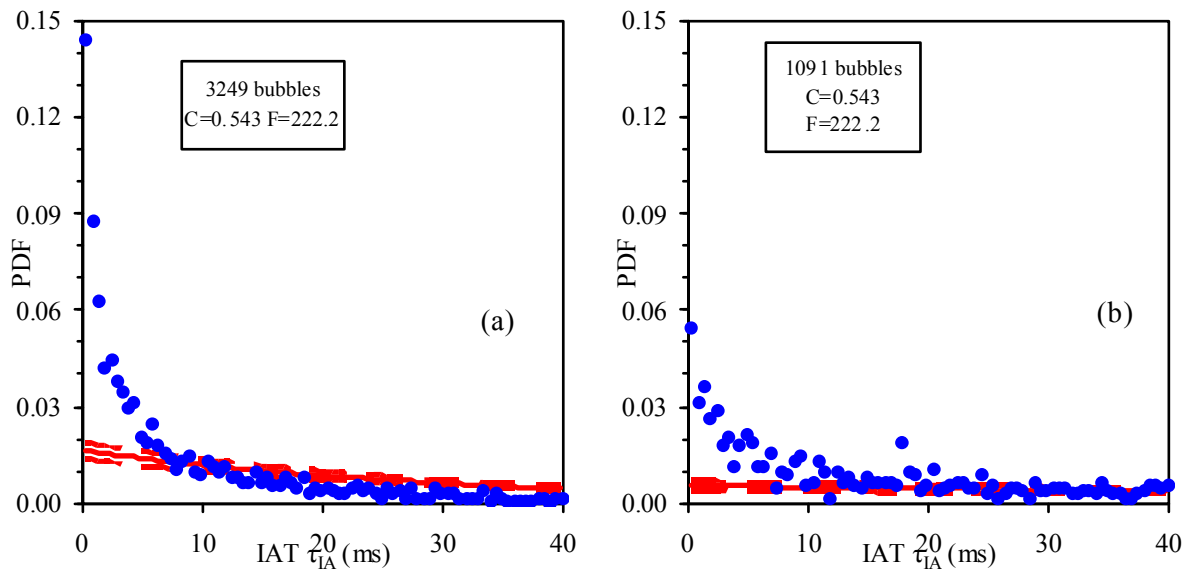


Fig. 7 – Interparticle arrival time analysis in the dropshaft at $x=150$ mm and $z=30$ mm. Class (a) 1 and (b) 3, (●) experimental data, (—) Poisson distribution, (dashed line) lower/upper range

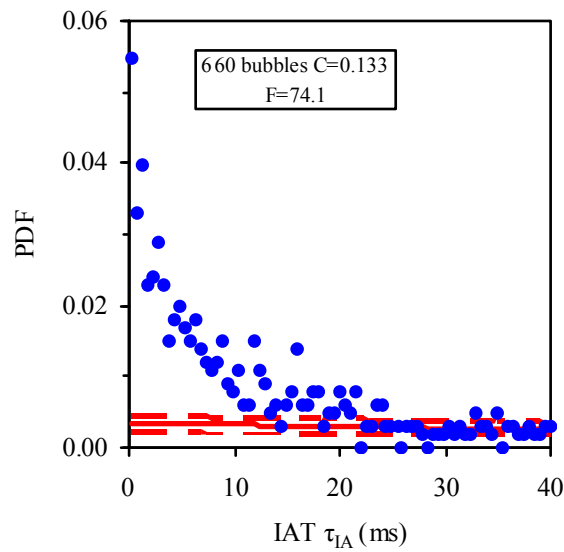


Fig. 8 – Interparticle arrival time analysis in the dropshaft at $x=115$ mm and $z=250$ mm. Class No. 1, (●) experimental data, (—) Poisson distribution, (dashed line) lower/upper range

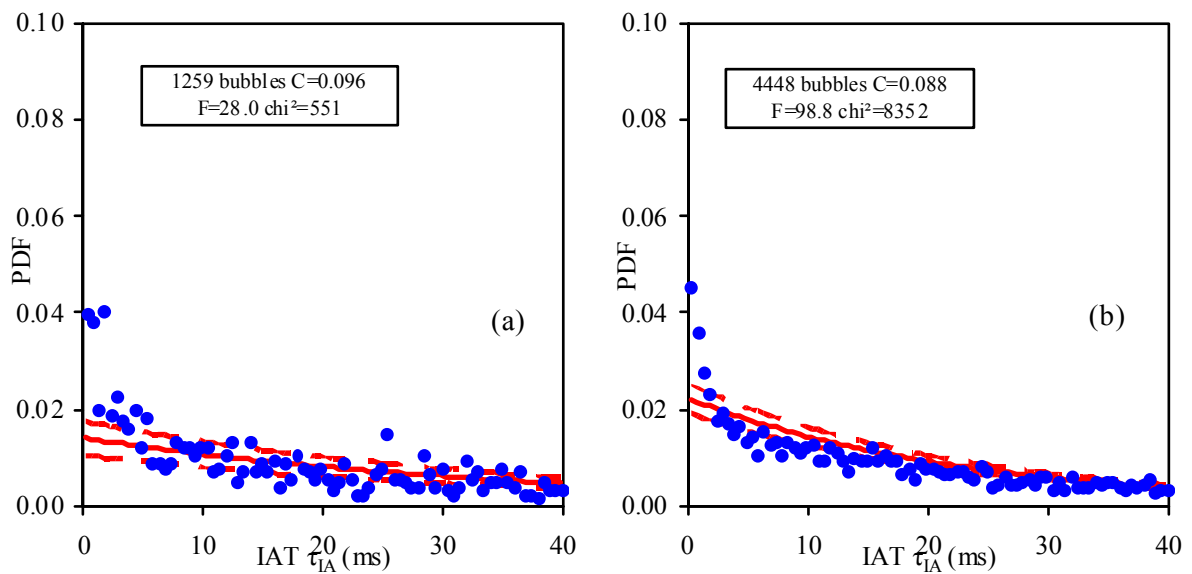


Fig. 9 – Interparticle arrival time analysis in the hydraulic jump at (a) $F_1=6.51$, $(x-x_1)/d_1=4.17$ and $y/d_1=1.596$ and (b) $F_1=10.8$, $(x-x_1)/d_1=3.91$ and $y/d_1=0.910$, (●) experimental data, (—) Poisson distribution, (dashed line) lower/upper range

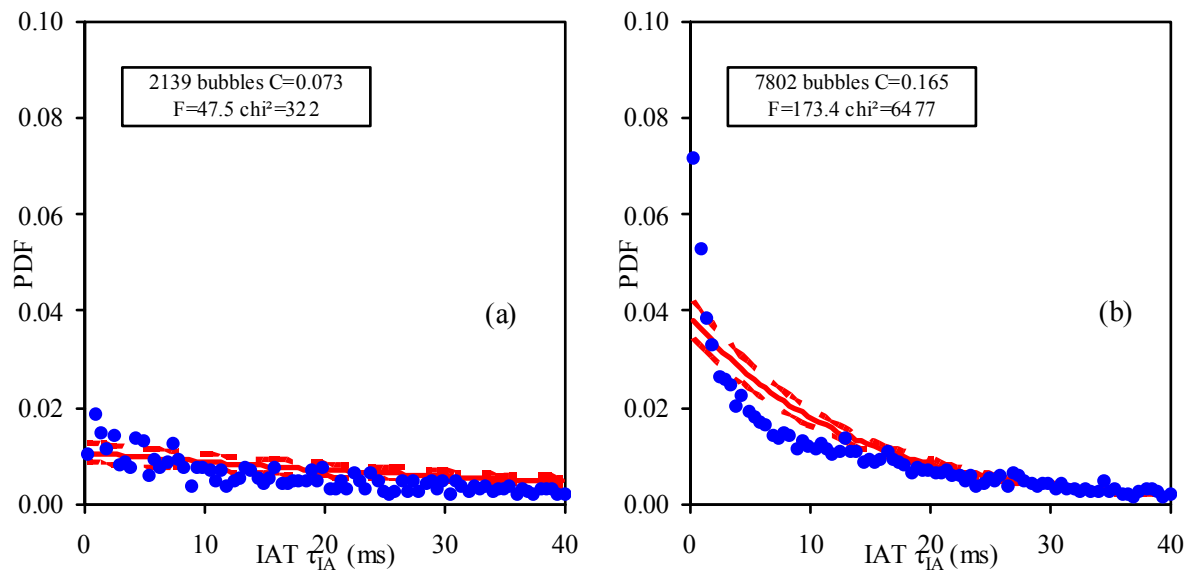


Fig. 10 – Interparticle arrival time analysis in the hydraulic jump at (a) $F_1=10.8$, $(x-x_1)/d_1=27.3$ and $y/d_1=3.254$ and (b) $F_1=14.3$, $(x-x_1)/d_1=4.20$ and $y/d_1=0.979$, (●) experimental data, (—) Poisson distribution, (dashed line) lower/upper range

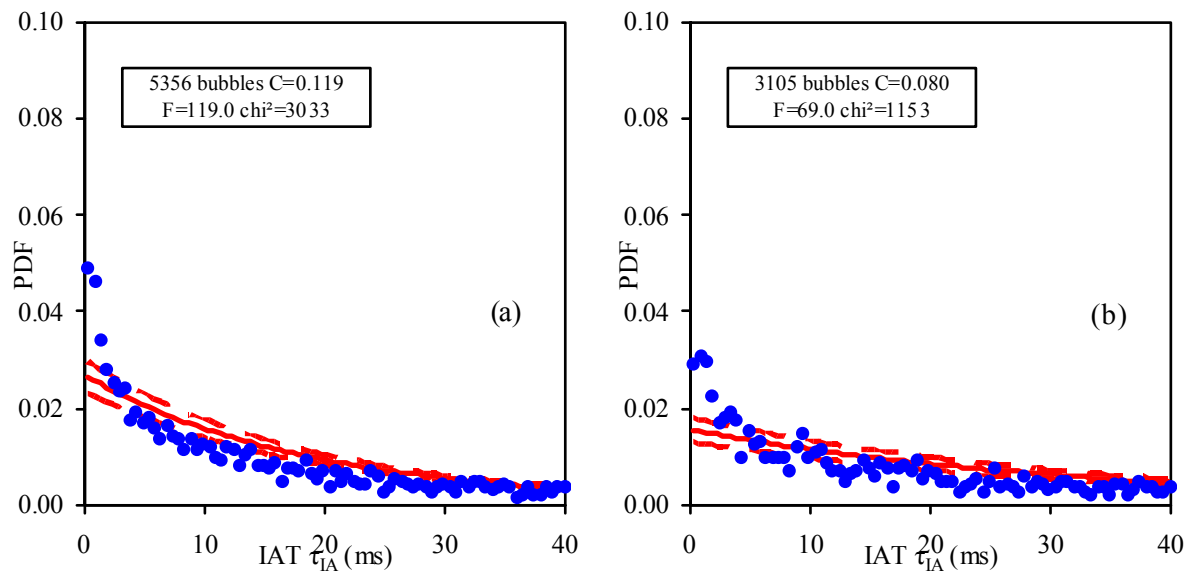


Fig. 11 – Interparticle arrival time analysis in the hydraulic jump at (a) $F_1=14.3$, $(x-x_1)/d_1=29.4$ and $y/d_1=2.239$ and (b) $F_1=14.3$, $(x-x_1)/d_1=42.0$ and $y/d_1=3.500$, (●) experimental data, (—) Poisson distribution, (dashed line) lower/upper range

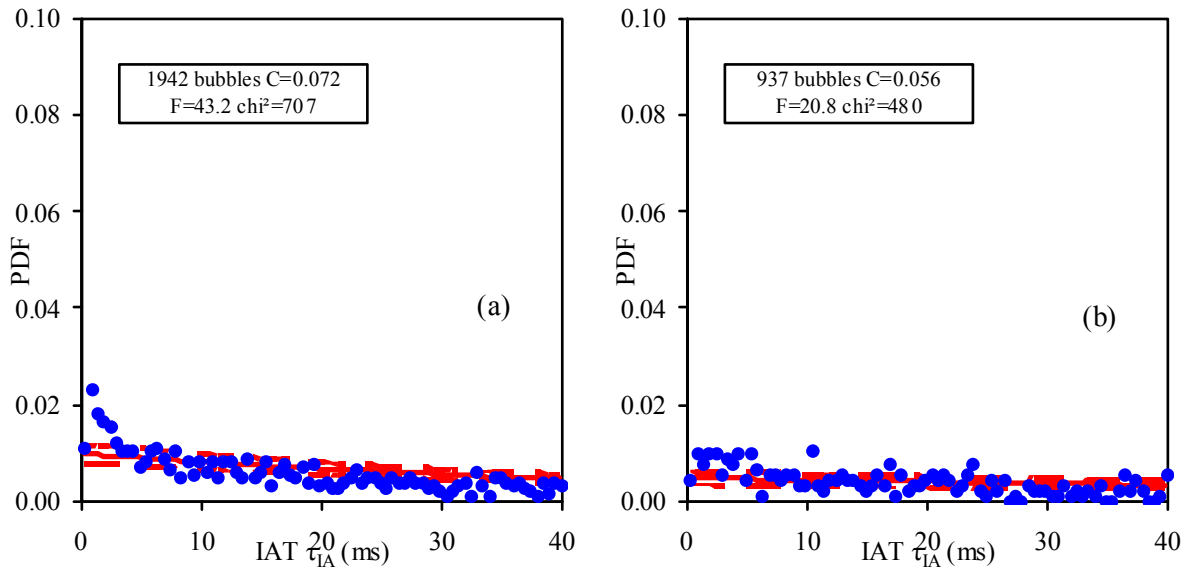


Fig. 12 – Interparticle arrival time analysis in the hydraulic jump at (a) $F_1=14.3$, $(x-x_1)/d_1=54.6$ and $y/d_1=5.601$ and (b) $F_1=14.3$, $(x-x_1)/d_1=54.6$ and $y/d_1=9.382$, (●) experimental data, (—) Poisson distribution, (dashed line) lower/upper range

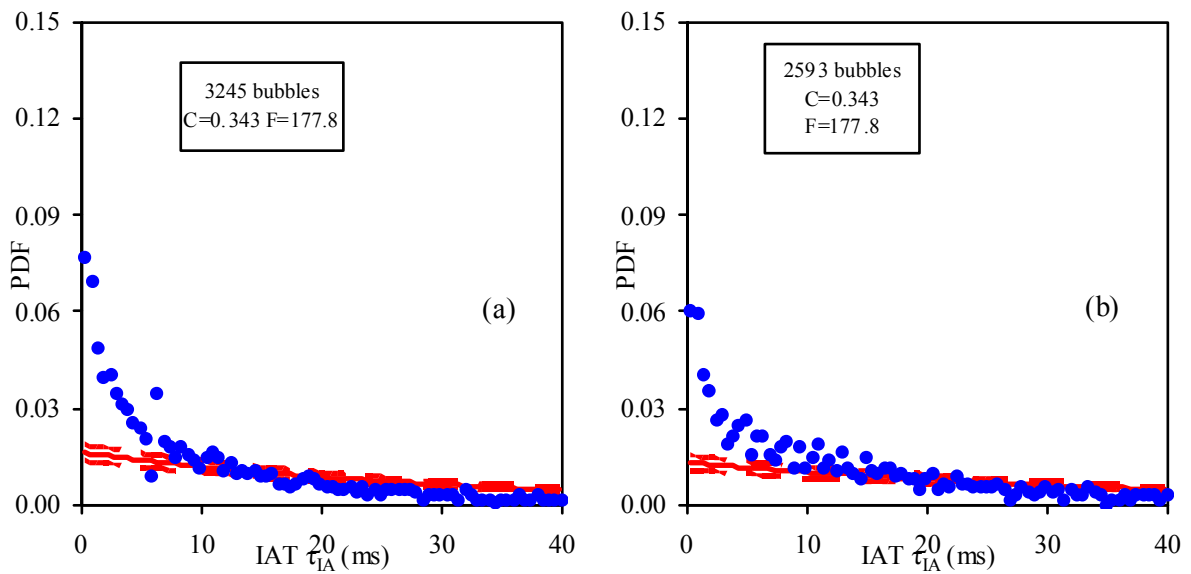


Fig. 13 – Interparticle arrival time analysis in the hydraulic jump for $F_1=14.3$ at $(x-x_1)/d_1=8.40$ and $y/d_1=1.399$. Class (a) 1 and (b) 2, (●) experimental data, (—) Poisson distribution, (dashed line) lower/upper range

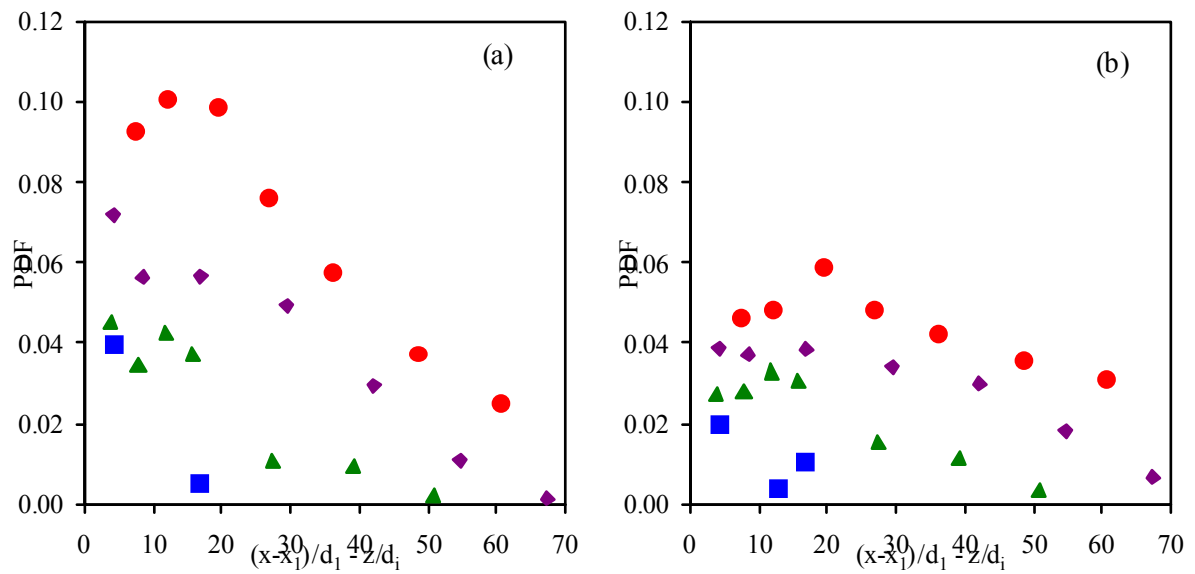


Fig. 14 – Distribution with the distance of the PDF for bubbles with τ_{IA} from 0 to 0.5 ms (a) and from 1.0 to 1.5 ms (b), (●) dropshaft, (■) hydraulic jump for $F_1=6.51$, (▲) hydraulic jump for $F_1=10.8$, (◆) hydraulic jump for $F_1=14.3$

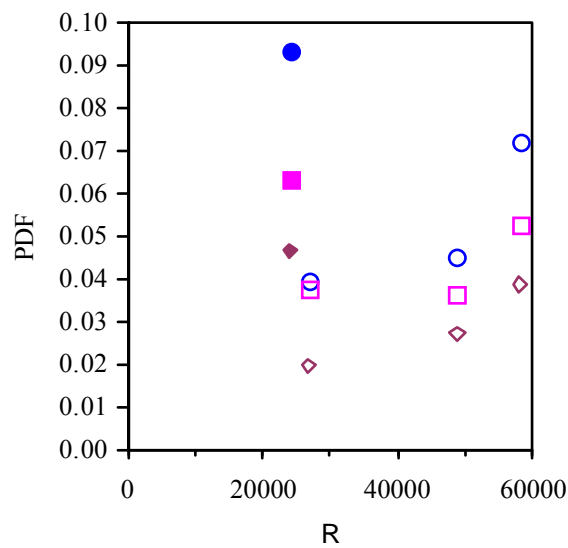


Fig. 15 – Distribution with R of the PDF in the dropshaft and in the hydraulic jump for bubbles with τ_{IA} from (● and ○) 0 to 0.5 ms (■ and □) from 0.5 to 1.0 ms and (◆ and ◇) from 1.0 to 1.5 ms